Parameter estimation in orthorhombic media using multicomponent reflection data

Vladimir Grechka*, Andres Pech† & Ilya Tsvankin†
*Shell International Exploration and Production, Houston, TX.
†Center for Wave Phenomena, Colorado School of Mines.

ABSTRACT

Orthorhombic media with a horizontal symmetry plane adequately describe seismic signatures recorded over many naturally fractured reservoirs. Here we show that for a range of orthorhombic models wide-azimuth traveltimes of PP and SS (the fast S_1 and slow S_2) reflections can be inverted for Tsvankin's anisotropic parameters and the azimuths of the vertical symmetry planes. If shear waves are not excited, SS traveltimes can be found in model-independent fashion from PP and PS (converted-wave) data, which makes the method applicable to offshore surveys.

The feasibility of parameter estimation is strongly dependent on reflector dip and orientation. For a horizontal reflector beneath a single orthorhombic layer, the vertical velocities and reflector depth cannot be found from reflection traveltimes in a unique fashion. If the reflector is dipping, the inversion is ambiguous when the dip plane is close to one of the vertical symmetry planes of the orthorhombic layer above it. For other azimuthal directions of a dipping reflector, the parameter estimation is possible in theory.

To perform velocity analysis for orthorhombic models composed of homogeneous layers separated by plane or curved interfaces, we apply multicomponent stacking-velocity tomography. The tomographic algorithm, which operates with the NMO ellipses, zero-offset traveltimes and reflection time slopes, is designed to estimate the interval anisotropic parameters and the shapes of the reflecting interfaces. Thus, multicomponent reflection data can be used to build the orthorhombic velocity model in the *depth* domain and carry out depth migration. Still, numerical tests show that for layered orthorhombic media it is preferable to have *a priori* knowledge of the vertical velocities to avoid instability in the inversion of noise-contaminated reflection data.

Key words: converted waves, orthorhombic media, parameter estimation

1 INTRODUCTION

Estimation of anisotropic velocity fields from reflection traveltimes of seismic waves is a nonlinear inverse problem that becomes increasingly more complicated for lower medium symmetries. The existence of a unique solution is determined by the reflection mode (PP, SS, PS, or a certain combination of them) being used, the available range of offsets and azimuths, and the reflector geometry.

For the simplest anisotropic model – transverse isotropy with a vertical symmetry axis (VTI) – PP-waves alone generally do not provide enough information for estimating Thomsen anisotropic coefficients ϵ and δ. If the VTI medium above the reflector is laterally homogeneous, PP traveltimes are fully controlled by the normal-moveout (NMO) velocity $V_{\rm nmo}(0)$ and the anellipticity coefficient η, rather than by the vertical P-wave velocity V_{P0}, ϵ, and δ individually (Alkhalifah and Tsvankin, 1995; Grechka and Tsvankin, 1998a,b). For a limited class of VTI models with dipping or curved interme-

diate interfaces it is possible to invert PP traveltimes for the interval values of V_{P0}, ϵ, and δ (Le Stunff et al., 2001; Grechka et al., 2002). Supplementing PP-wave data with converted PSV-waves overcomes the ambiguity in the moveout inversion, provided the reflector has mild dip (Tsvankin and Grechka, 2000a,b). It is even more beneficial to combine PP and PS (in general, there are two split converted waves – PS_1 and PS_2) data in parameter estimation for lower-symmetry models, such as orthorhombic and monoclinic (Grechka, Theophanis and Tsvankin, 1999; Grechka, Contreras and Tsvankin, 2000).

Unfortunately, processing of converted waves is complicated by a number of practical problems related to polarity reversals, significant conversion-point dispersal, and the asymmetry of PS-wave moveout on common-midpoint (CMP) and common-conversion-point (CCP) gathers. In particular, asymmetric PS moveout (see the discussion of "diodic" velocity in Thomsen, 1999) cannot be treated by velocity-analysis algorithms based on the conventional hyperbolic moveout equation. These difficulties in converted-wave processing can be overcome using a method proposed by Grechka and Tsvankin (2001). They showed that the traveltimes of PP and PS reflections from a certain interface can be combined to obtain the traveltimes of pure (nonconverted) SS-waves for the same reflector. Most importantly, SS traveltimes are computed without using any velocity information, so the whole procedure can be performed prior to velocity analysis (although correlation of PP- and PS reflections is required). Then one can estimate SS-wave normal-moveout (NMO) velocities (in 2-D) or NMO ellipses (in 3-D) and use them, along with PP data, in anisotropic parameter estimation.

A practical velocity-analysis algorithm based on these ideas was suggested for transversely isotropic media by Grechka, Pech and Tsvankin (2001). They used the NMO velocities (or ellipses in 3-D), zero-offset traveltimes, and reflection time slopes of PP- and $SS(SVSV)$-waves (SS traveltimes found from PP and PS data) in a tomographic algorithm capable of estimating the interval anisotropic parameters and the shapes of interfaces for TI media with a vertical and tilted axis of symmetry. Grechka, Tsvankin, Bakulin, and Hansen (2001) successfully applied this methodology to anisotropic parameter estimation at the Siri reservoir in the North Sea.

Here, we extend the approach of Grechka, Pech and Tsvankin (2001) to more complicated orthorhombic media believed to be typical for naturally fractured oil and gas reservoirs (Schoenberg and Helbig, 1997; Bakulin et al., 2000). Our analysis shows that wide-azimuth reflection traveltimes of PP-waves and two split converted waves (PS_1 and PS_2) are sufficient for constraining the anisotropic parameters of a relatively wide range of orthorhombic models. First, we establish the conditions that make it possible to estimate the vertical velocities and Tsvankin's (1997) anisotropic coefficients of a single dipping orthorhombic layer and, therefore, fully reconstruct this model in the depth domain. Then we proceed with parameter estimation for orthorhombic media composed of multiple homogeneous layers separated by plane or curved interfaces. Numerical tests indicate that although for a certain class of such layered models the inversion of multicomponent data is theoretically possible, it may not be sufficiently stable. *A priori* knowledge of the vertical velocities helps to reduce the errors in the estimated anisotropic coefficients to values of about 0.05–0.1.

2 TOMOGRAPHIC PARAMETER ESTIMATION USING MULTICOMPONENT DATA

The success of the parameter-estimation procedure discussed below depends on our ability to construct SS traveltimes from PP and PS reflection data using the method of Grechka and Tsvankin (2001). Although this method requires no explicit velocity information, one must be able to pick traveltimes of PP- and PS-waves on prestack common-receiver gathers. Traveltime picking, however, may be difficult for traces with low PS amplitudes (and, correspondingly, low signal-to-noise ratio) caused by small reflection coefficients in areas of polarity reversals. To evaluate the seriousness of this issue for a typical moderately anisotropic orthorhombic model, we use a synthetic test.

Multicomponent seismograms in Figure 1 are computed by anisotropic dynamic ray tracing. As expected, the PP reflection has the highest amplitude on the vertical component (Figure 1d), whereas the two split converted waves PS_1 and PS_2 are clearly seen on the horizontal inline and crossline components (Figures 1b, c). Despite some dimming of the PS_1- and PS_2-waves at certain azimuths, the offset range of those low-amplitude arrivals is relatively narrow. Therefore, Figures 1b, c suggest that, despite the presence of polarity reversals, picking of wide-azimuth converted-wave traveltimes over orthorhombic media is quite feasible. This conclusion remains valid for media with a smaller shear-wave splitting coefficient than those used here, where the PS_1 and PS_2 arrivals overlap, and time picking has to be preceded by Alford (1986) rotation.

Once the traveltimes of PP-, PS_1-, and PS_2-waves have been picked, the method of Grechka and Tsvankin

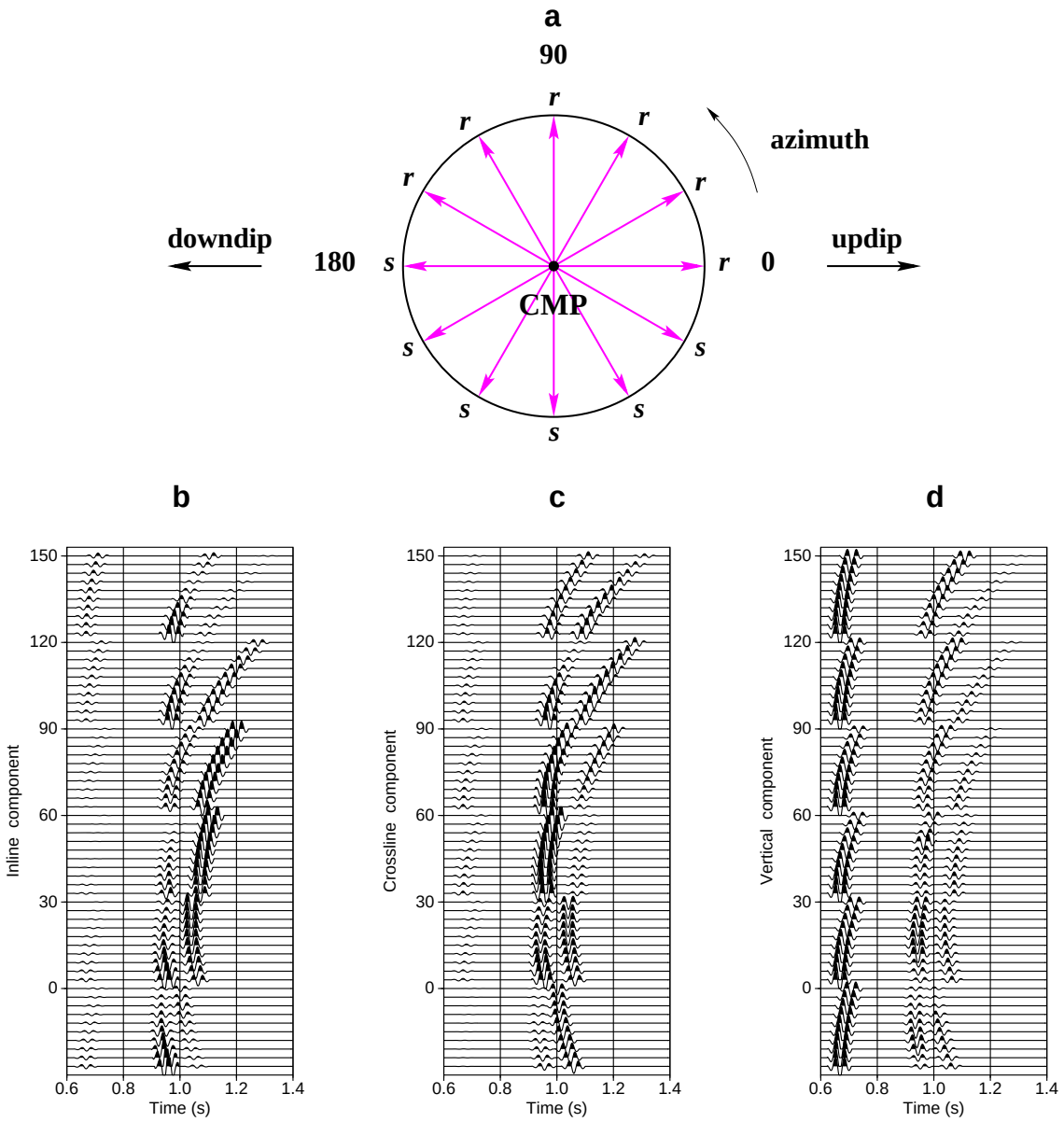

Figure 1. (a) Plan view of a multiazimuth CMP gather, with sources for each line located on one side marked by s, and receivers on the side marked by r. (b-d) True-amplitude three-component synthetic seismograms of PP-, PS_1- and PS_2-waves reflected from a dipping interface beneath an orthorhombic layer. The numbers 0, 30, 60, 90, 120, and 150 on the vertical axis in Figures (b-d) indicate the azimuth (in degrees) of the block of traces plotted under this number (e.g., all traces between numbers 150 and 120 have an azimuth of 150°). The source-receiver offsets within each block of traces change from 0.1 km to 1 km in 0.1 km increments. The azimuth of the dip plane is $\psi = 0°$ (see the plan view), the dip $\phi = 30°$, and the depth under the common midpoint $z = 1$ km. The azimuth of the vertical $[x_1, x_3]$ symmetry plane of the orthorhombic layer with respect to the reflector dip plane is $\beta = 60°$. Tsvankin's (1997) anisotropic parameters of the layer are $V_{P0} = 2.9$ km/s, $V_{S0} = 1.4$ km/s, $\epsilon^{(2)} = 0.15$, $\delta^{(2)} = 0.05$, $\gamma^{(2)} = -0.25$, $\epsilon^{(1)} = 0.25$, $\delta^{(1)} = 0.15$, $\gamma^{(1)} = -0.20$, $\delta^{(3)} = -0.05$.

(2001) can be employed to compute the traveltimes t_{S1} and t_{S2} of pure shear-wave reflections S_1S_1 and S_2S_2 from the same interface. The traveltimes t_{S1} and t_{S2} are guaranteed to be symmetric with respect to the common midpoint, so they can be processed by means of hyperbolic semblance analysis. For wide-azimuth data, it is possible to reconstruct the NMO ellipses of both PP- and SS-waves using a 3-D hyperbolic semblance operator (Grechka and Tsvankin, 1999b).

The NMO ellipses, along with the corresponding

horizontal projections of the slowness vectors $\boldsymbol{p}_Q$ (the reflection slopes on zero-offset time sections) and zero-offset traveltimes τ_Q ($Q = P$, S_1, or S_2), are used as the input data for anisotropic stacking-velocity tomography. The data vector for an N-layered orthorhombic medium is

$$\boldsymbol{d}(Q, \boldsymbol{Y}, n) \equiv \{\tau_Q(\boldsymbol{Y}, n), \boldsymbol{p}_Q(\boldsymbol{Y}, n), \boldsymbol{W}_Q(\boldsymbol{Y}, n)\}, \quad (1)$$

where $\boldsymbol{Y} = [Y_1, Y_2]$ is the CMP location, $n = 1, 2, ..., N$ is the reflector number and $\boldsymbol{W}$ is the 2×2 matrix (Grechka and Tsvankin, 1998b) describing the NMO ellipse.

Stacking-velocity tomography for multicomponent data is described in detail by Grechka, Pech and Tsvankin (2001). The main advantages of restricting the inversion to the hyperbolic portion of reflection moveout is high computational efficiency (only one zero-offset ray for each reflection event needs to be traced) and the analytic insight into constrained parameter combinations provided by the NMO ellipses. The tomographic algorithm is based on a two-step procedure for estimating the model vector $\boldsymbol{m}$ that contains the interval parameters of orthorhombic media and the coefficients of the polynomials specifying the model interfaces. For a given set of trial interval anisotropic parameters, the zero-offset traveltimes and reflection slopes are used to compute the one-way zero-offset rays and reconstruct the medium interfaces (i.e., build the trial model in depth). Then the interval parameters are obtained by minimizing the differences between the computed and measured NMO ellipses $\boldsymbol{W}$ for all available reflection events.

In the next section, we discuss the issues of uniqueness and stability in the inversion of the data vector (1) for the parameters of orthorhombic media.

3 PARAMETER ESTIMATION IN A SINGLE ORTHORHOMBIC LAYER

First, we review notation and some relevant properties of wave propagation for orthorhombic models. Seismic signatures in orthorhombic media can be conveniently described in terms of the two vertical velocities,

$$V_{P0} = \sqrt{\frac{c_{33}}{\rho}} \quad \text{and} \quad V_{S0} = \sqrt{\frac{c_{55}}{\rho}}, \quad (2)$$

and Thomsen-style anisotropic coefficients $\epsilon^{(1,2)}$, $\delta^{(1,2,3)}$, and $\gamma^{(1,2)}$ introduced by Tsvankin (1997); c_{ij} are the components of the stiffness tensor and ρ is the density. The coefficients $\epsilon^{(i)}$, $\delta^{(i)}$, $\gamma^{(i)}$ ($i = 1, 2$) defined in the vertical symmetry planes $[x_2, x_3]$ and $[x_1, x_3]$ (Figure 2) have the same meaning as Thomsen's (1986) parameters ϵ, δ, and γ for transverse isotropy. The coefficient $\delta^{(3)}$ plays the role of Thomsen's δ in the horizontal plane $[x_1, x_2]$.

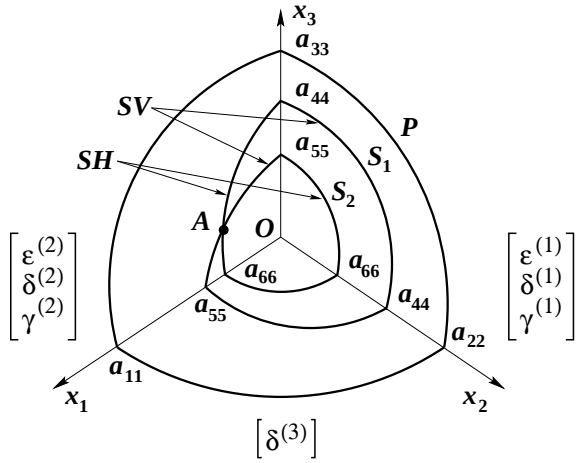

Figure 2. Sketch of body-wave phase-velocity surfaces in orthorhombic media (after Grechka, Theophanis and Tsvankin, 1999). The coefficients $\epsilon^{(1)}$, $\delta^{(1)}$ and $\gamma^{(1)}$ are defined in the symmetry plane $[x_2, x_3]$, while $\epsilon^{(2)}$, $\delta^{(2)}$ and $\gamma^{(2)}$ correspond to the plane $[x_1, x_3]$ (Tsvankin, 1997). $a_{ij} \equiv \sqrt{c_{ij}/\rho}$, where c_{ij} are the stiffness coefficients and ρ is the density.

The kinematics of wave propagation in the symmetry planes of orthorhombic media is practically identical to that in VTI media. The only notable difference is caused by the so-called singularity directions in orthorhombic media (the point A in Figure 2), where the phase velocities of two shear waves coincide. The S_2-wavefront near a singularity usually becomes multivalued, while the wavefront of the fast S_1-wave develops an elliptical hole. Those complicated phenomena are outside of the scope of this paper; hereafter, we assume that the singularities are located outside of the fan of ray directions used for velocity analysis.

3.1 Horizontal reflector

The semi-axes of NMO ellipses for all reflection modes in a horizontal orthorhombic layer are co-oriented with the vertical symmetry planes and have the following simple form (Grechka, Theophanis and Tsvankin, 1999):

$$\frac{1}{V^2_{Q,\mathrm{nmo}}(\alpha)} = \frac{\cos^2\alpha}{\left[V^{(2)}_{Q,\mathrm{nmo}}\right]^2} + \frac{\sin^2\alpha}{\left[V^{(1)}_{Q,\mathrm{nmo}}\right]^2} \quad (3)$$

($Q = P$, S_1, or S_2);

α is the azimuth with respect to the $[x_1, x_3]$-plane. Because of the kinematic equivalence between the symmetry planes of orthorhombic and VTI media, the semi-axes of the NMO ellipses ($V^{(i)}_{Q,\mathrm{nmo}}$) can be obtained by adapting the VTI equations (Grechka and Tsvankin, 1998b)

$$V^{(2)}_{P,\mathrm{nmo}} = V_{P0}\sqrt{1+2\,\delta^{(2)}}\,, \tag{4}$$

$$V^{(1)}_{P,\mathrm{nmo}} = V_{P0}\sqrt{1+2\,\delta^{(1)}}\,, \tag{5}$$

$$V^{(2)}_{S1,\,\mathrm{nmo}} = V_{S1}\sqrt{1+2\,\gamma^{(2)}} = \sqrt{c_{66}/\rho}\,, \tag{6}$$

$$V^{(1)}_{S1,\,\mathrm{nmo}} = V_{S1}\sqrt{1+2\,\sigma^{(1)}}\,, \tag{7}$$

$$V^{(2)}_{S2,\,\mathrm{nmo}} = V_{S2}\sqrt{1+2\,\sigma^{(2)}}\,, \tag{8}$$

$$V^{(1)}_{S2,\,\mathrm{nmo}} = V_{S2}\sqrt{1+2\,\gamma^{(1)}} = \sqrt{c_{66}/\rho}\,, \tag{9}$$

where

$$\sigma^{(2)} = \left(\frac{V_{P0}}{V_{S2}}\right)^2 \left(\epsilon^{(2)} - \delta^{(2)}\right)\,,$$

$$\sigma^{(1)} = \left(\frac{V_{P0}}{V_{S1}}\right)^2 \left(\epsilon^{(1)} - \delta^{(1)}\right)\,, \tag{10}$$

and

$$V_{S2} = V_{S0}\,, \qquad V_{S1} = V_{S0}\sqrt{\frac{1+2\,\gamma^{(1)}}{1+2\,\gamma^{(2)}}} \tag{11}$$

Here, it is assumed that the fast mode S_1 at vertical incidence is polarized in the x_2-direction.

As follows from equations (4)–(11), the anisotropic coefficients $\epsilon^{(1,2)}$, $\delta^{(1,2)}$ and $\gamma^{(1,2)}$ can be estimated in a unique fashion only if either one of the vertical velocities or the reflector depth is known. This result is hardly surprising because the NMO velocities and zero-offset traveltimes cannot be unambiguously inverted for the anisotropic parameters even for the higher-symmetry horizontal VTI layer.

Note that the coefficient $\delta^{(3)}$ has no influence on the NMO ellipses in a horizontal layer and, therefore, cannot be determined from conventional-spread reflection moveout. A more detailed discussion of the NMO ellipses of pure and converted waves in horizontally layered orthorhombic media, and their inversion, can be found in Grechka, Theophanis and Tsvankin (1999).

3.2 Plane dipping reflector co-oriented with a vertical symmetry plane

While moveout inversion of multicomponent data is nonunique for a horizontal VTI layer, Tsvankin and Grechka (2000a,b) and Grechka, Pech and Tsvankin (2001a) showed that the vertical velocities and coefficients ϵ and δ can be estimated uniquely from PP and SS traveltimes if the reflector beneath the VTI medium has a mild dip of at least 15-20°. Here, we examine whether or not this result holds for an orthorhombic layer above a plane dipping reflector that is oriented in such a way that the dip plane coincides with one of the vertical symmetry planes of the overburden.

Suppose the dip plane of the reflector represents the $[x_1,\, x_3]$ symmetry plane of the orthorhombic medium. Since the slowness vector of the zero-offset ray for any pure mode is orthogonal to the reflector, the horizontal slowness projection at zero offset is confined to the dip plane. Both horizontal slowness components (p_1 and p_2) of the zero-offset ray can be found from reflection slopes on the zero-offset (or stacked) time section. Therefore, reflection time slopes can be used to find the azimuthal direction of both the reflector and the $[x_1,\, x_3]$ symmetry plane.

Then, the model vector $\boldsymbol{m}$ to be estimated from moveout data contains the remaining eleven unknowns: nine Tsvankin's (1997) parameters discussed above (V_{P0}, V_{S0}, $\epsilon^{(1)}$, $\epsilon^{(2)}$, $\delta^{(1)}$, $\delta^{(2)}$, $\delta^{(3)}$, $\gamma^{(1)}$, and $\gamma^{(2)}$), the reflector dip ϕ, and the distance D between the reflector and the origin of the Cartesian coordinate system $\boldsymbol{O}$. The elements of $\boldsymbol{m}$ are supposed to be found from the eighteen-component data vector (1) that has six zero elements,

$$p_{2,\,Q} = 0 \quad \text{and} \quad W_{12,\,Q} = 0 \tag{12}$$

$$(Q = P,\ S_1,\ \text{or}\ S_2)\,,$$

because $[x_1,\, x_3]$ is the symmetry plane for the whole model. The remaining three zero-offset traveltimes τ_Q, three horizontal slownesses $p_{1,\,Q}$ and six diagonal elements of the matrices $\boldsymbol{W}_Q$ (which correspond to the dip- and strike-components of the NMO velocities) provide a total of 12 equations.

However, below we demonstrate that the expressions for the traveltimes τ_Q are not independent. The equation of a planar reflector can be written as

$$\boldsymbol{n}\cdot\boldsymbol{x} = D\,, \tag{13}$$

where $\boldsymbol{n} \equiv [\sin\phi,\, 0,\, \cos\phi]$ is a unit vector perpendicular to the reflector. Assuming that the origin $\boldsymbol{O}$ of the Cartesian coordinate system is placed at the common midpoint, the reflection point $\boldsymbol{r}_Q$ of the zero-offset ray can be found from

$$\boldsymbol{r}_Q = \boldsymbol{g}_Q\,\tau_Q\,, \tag{14}$$

where $\boldsymbol{g}_Q$ is the group-velocity vector of mode Q. Since the point $\boldsymbol{r}_Q$ lies on the reflector (13), the one-way zero-offset traveltime is

$$\tau_Q = \frac{D}{\boldsymbol{n}\cdot\boldsymbol{g}_Q}\,. \tag{15}$$

Snell's law requires that the slowness vectors $\boldsymbol{p}_Q \equiv [p_{1,\,Q},\, 0,\, p_{3,\,Q}]$ of pure modes be parallel to each other and orthogonal to the reflector, so

$$\boldsymbol{n} = \frac{\boldsymbol{p}_Q}{|\boldsymbol{p}_Q|} \qquad (Q = P,\ S_1,\ \text{or}\ S_2)\,. \tag{16}$$

Combining equations (15) and (16) and taking into account that $\boldsymbol{p}_Q\cdot\boldsymbol{g}_Q = 1$ (this equality plays the role of

eikonal equation in anisotropic media) yields

$$\tau_Q = \frac{D\,|\boldsymbol{p}_Q|}{\boldsymbol{p}_Q \cdot \boldsymbol{g}_Q} = D\,|\boldsymbol{p}_Q| = \frac{D\,p_{1,Q}}{\sin\phi} \tag{17}$$

$(Q = P,\ S_1,\ \text{or}\ S_2)$.

Equation (17) shows that three zero-offset traveltimes τ_P, τ_{S1}, and τ_{S2} constrain only *one* combination of the model parameters – $D/\sin\phi$. Therefore, the number of independent equations to be solved for the 11 unknown parameters reduces from 12 to 10. Clearly, this inverse problem does not have a unique solution.

3.3 Arbitrarily oriented plane dipping reflector

If the dip plane of the reflector does not coincide with either vertical symmetry plane, each NMO ellipse generally has a different orientation. That increases the number of independent components of the data vector (1) and, as demonstrated below, can make the inversion unambiguous.

Indeed, if the dip plane and the symmetry planes are misaligned, the number of equations exceeds the number of unknowns. The model vector includes 13 elements to be found from the data:

$$\begin{aligned}\boldsymbol{m} \;=\; &\{V_{P0},\, V_{S0},\, \epsilon^{(1)},\, \delta^{(1)},\, \gamma^{(1)},\, \epsilon^{(2)},\, \delta^{(2)},\, \gamma^{(2)},\\ &\delta^{(3)},\, \beta,\, D,\, \phi,\, \psi\},\end{aligned} \tag{18}$$

where β is the azimuth of the vertical symmetry plane $[x_1,\, x_3]$ and ψ is the azimuth of the dip plane of the reflector. The original number of equations (i.e., the number of measured quantities) is 18 [equation (1)], but, as discussed above [see equation (17)], the three traveltimes τ_Q provide only one independent equation. In addition, the ratio of the horizontal slowness components for each mode is fixed by the reflector azimuth ($p_{2,Q}/p_{1,Q} = \tan\psi$), which eliminates two more independent equations. Even with these factors taken into account, however, the number of equations (14) is larger than the number of unknown model parameters (13), and, in principle, the moveout inversion may be possible.

Still, the inverse problem is nonlinear, and the feasibility of parameter estimation has to be assessed by numerical testing on noise-contaminated data. Our numerical analysis shows that the inversion for a range of typical orthorhombic models is not only unique but also quite stable. Because of the multimodal nature of the misfit function, we perform several inversions starting from different points in the model space. The results in Figure 3 are obtained from the data $\boldsymbol{d} = \{\tau_Q,\, \boldsymbol{p}_Q,\, \boldsymbol{W}_Q\}$ generated for all three modes (P, S_1 and S_2) at a single CMP location. The traveltimes τ_Q, the horizontal slowness components $\boldsymbol{p}_Q$, and the NMO ellipses $\boldsymbol{W}_Q$ were contaminated by Gaussian noise with standard deviations of 1% for τ_Q and $\boldsymbol{p}_Q$ and 2% for $\boldsymbol{W}_Q$. In terms of anisotropic parameter estimation, these values of standard deviations are reasonable.

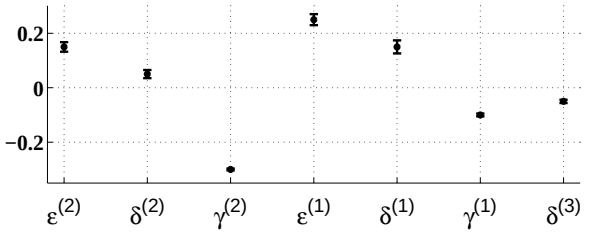

Figure 3. Inversion results for a single orthorhombic layer above a dipping reflector. The exact values of the anisotropic coefficients are marked by the dots; the bars correspond to the ± standard deviation in each parameter. The reflector dip ϕ is 30°, the azimuth of the dip plane $\psi = 0°$, and the azimuth of the $[x_1,\, x_3]$ symmetry plane of the layer $\beta = 60°$.

The parameter estimation was repeated 100 times for different realizations of the noise using a nonlinear least-squares algorithm. The maximum standard deviation in the recovered anisotropic coefficients does not exceed 0.025 (the value for $\delta^{(1)}$ in Figure 3), which means that the inversion is sufficiently stable. The standard deviations for the parameters not displayed in Figure 3 are small as well (1.2% and 0.6% for the vertical velocities V_{P0} and V_{S0}, respectively, and less than 1° for the angles β, ϕ and ψ).

For the model from Figure 3, the dip plane of the reflector deviates by 30° from the nearest vertical symmetry plane, which ensures the high stability of the inversion result. Figure 4 shows the inversion output for a model similar to that in Figure 3, but the azimuth angle between the dip plane and a vertical symmetry plane is just 15°, and the dip ϕ is reduced from 30° to 20°. Both changes have a negative influence on the performance of the inversion algorithm, and the error bars for most parameters become noticeably longer. Still, the moderate magnitude of the standard deviations indicates that the inversion remains sufficiently stable for practical applications.

Further reduction in the difference $|\psi - \beta|$ or in the reflector dip leads to a rapid increase in the errors (i.e., the standard deviations). Indeed, the analysis in the previous section suggests that the inversion becomes nonunique when $|\psi - \beta|$ approaches $k\,\pi/2$, where k is an integer. Likewise, the inversion becomes unstable if the reflector dip $\phi < 15°$, and for subhorizontal reflectors the anisotropic coefficients cannot be estimated without *a priori* knowledge of the vertical velocities or reflector

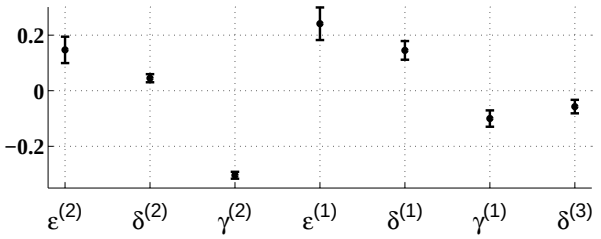

Figure 4. Same as Figure 3, but the reflector dip ϕ is 20°, and the azimuth of the $[x_1, x_3]$ symmetry plane $\beta = 15°$ (the azimuth of the dip plane remains $\psi = 0°$). The standard deviations for the parameters not shown on the plot are as follows: 1.3% and 0.7% for the velocities V_{P0} and V_{S0}, respectively, and less than 1.5° for the angles β, ϕ and ψ.

depth (see above). A similar dependence of the quality of moveout-inversion results on reflector dip was found for VTI media by Tsvankin and Grechka (2000a,b) and Grechka, Pech and Tsvankin (2001).

3.4 Curved reflector

If the reflector beneath an orthorhombic layer has arbitrary spatially varying curvature, the uniqueness of the inversion procedure is much more difficult to evaluate analytically. The feasibility of estimating the medium parameters in this case strongly depends on the shape and parameterization of the reflector and the spatial distribution of the common midpoints. Grechka et al. (2002) discussed those issues for stacking-velocity tomography of P-waves in VTI media.

Extensive testing on synthetic traveltimes shows that reflector curvature does not pose any serious problems for the parameter estimation in a single orthorhombic layer, provided the reflecting interface contains dips over 15° and the dip directions deviate from the vertical symmetry planes. Typical inversion results for noise-contaminated data τ_Q, $\boldsymbol{p}_Q$ and $\boldsymbol{W}_Q$ from nine CMP locations are displayed in Figure 5. As in the previous test, the inversion was repeated 100 times to study the distribution of the estimated parameters. The standard deviations in Figure 5b are even smaller than those in Figure 3; this conclusion also holds for the vertical velocities V_{P0}, V_{S0} and the reflector orientation (not shown).

The increase in stability for the curved reflector in Figure 5 is explained by the relatively wide range of reflector dips and azimuths sampled by the zero-offset rays. In other words, each CMP provides independent information. This advantage of curved interfaces, of course, can be fully exploited only if it is still possible to treat the medium above the reflector as homogeneous.

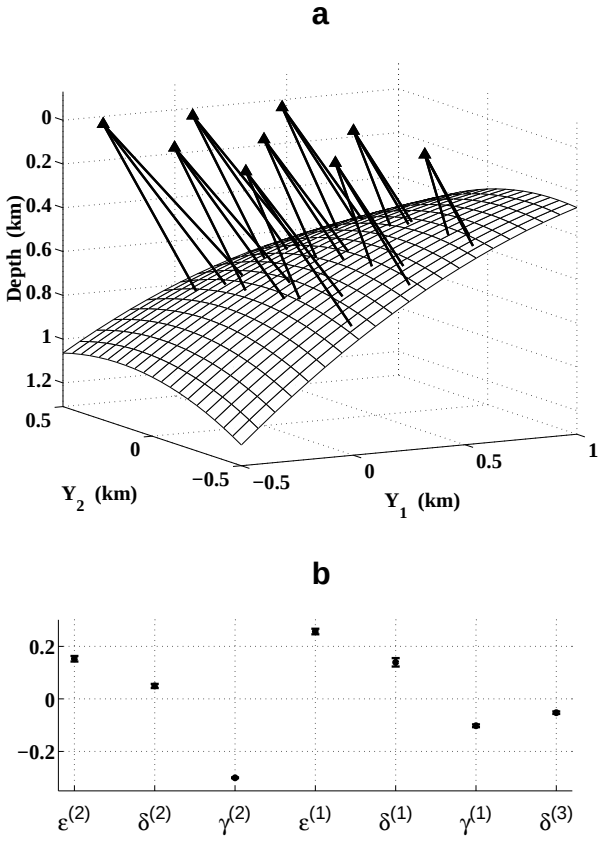

Figure 5. (a) Zero-offset rays of the P- S_1- and S_2-waves reflected from a curved interface below an orthorhombic layer and (b) the estimated anisotropic parameters. The $[x_1, x_3]$ symmetry plane makes an angle of 60° with the Y_1-axis. The data were contaminated with Gaussian noise that had the same standard deviations as in Figure 3. The exact values of the anisotropic coefficients are marked by the dots, while the bars correspond to the ± standard deviation in each parameter.

4 STACKING-VELOCITY TOMOGRAPHY IN LAYERED MEDIA

The above analysis for a single orthorhombic layer helped to reveal the potential of the multicomponent inversion algorithm. In this section, the methodology of stacking-velocity tomography is applied to more realistic models composed of homogeneous orthorhombic layers separated by plane or curved interfaces.

If *noise-free* data $\{\tau_Q, \boldsymbol{p}_Q, \boldsymbol{W}_Q\}$ ($Q = P, S_1, S_2$) for all interfaces are available, and the reflectors satisfy the conditions established for a single layer (i.e., the dips exceed 15-20° and the reflector azimuths sufficiently deviate from those of the vertical symmetry planes), the tomographic algorithm can recover the interval orthorhombic parameters along with the shapes of the interfaces. However, due to error accumulation with depth and a

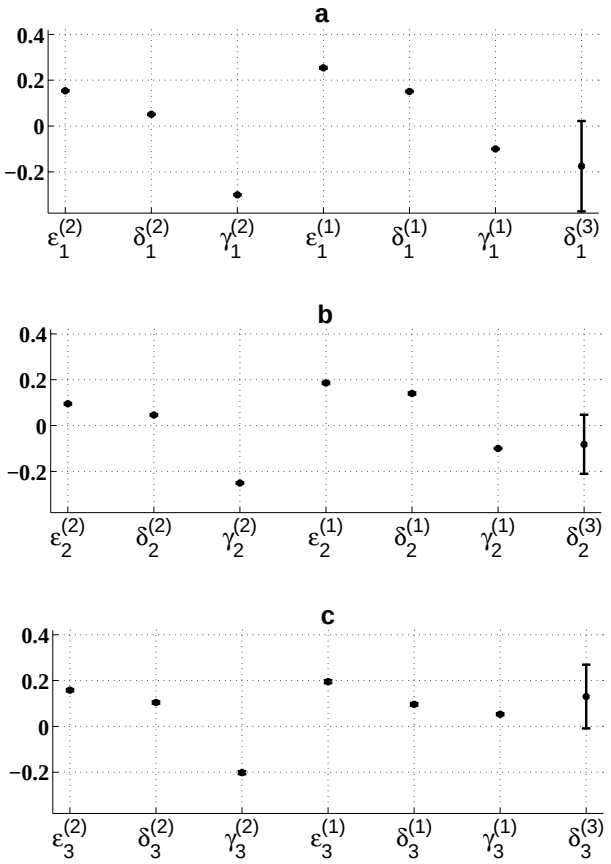

Figure 6. The results of stacking-velocity tomography for a model composed of three horizontal layers (a – top layer, b – middle layer, c – bottom layer) with different azimuths of the vertical symmetry planes. The vertical velocities were assumed to be known; from top to bottom, $V_{P0,1} = 1.0$ km/s, $V_{S0,1} = 0.5$ km/s, $V_{P0,2} = 1.5$ km/s, $V_{S0,2} = 0.6$ km/s, and $V_{P0,3} = 1.8$ km/s, $V_{S0,3} = 1.0$ km/s. The layer thicknesses are $z_1 = 0.4$ km, $z_2 = 0.6$ km and $z_3 = 0.8$ km, and the azimuths of the symmetry planes are $\beta_1 = 40°$, $\beta_2 = 70°$ and $\beta_3 = 10°$.

lower sensitivity of surface data to the parameters of deeper layers (e.g., Grechka et al., 2002), even moderate noise causes substantial errors in the interval parameters.

To make the inversion sufficiently stable for field-data applications, we assume that the interval vertical velocities $V_{P0,n}$ or $V_{S0,n}$) are known in all layers $n = 1, \ldots, N$; alternatively, it is possible to specify the thickness of each layer. Such an assumption may not be too restrictive in reservoir characterization because seismic inversion for orthorhombic anisotropy would typically be performed at later stages of the reservoir development when borehole and check-shot data are already available.

Figure 6 shows the parameter-estimation results for a model composed of three horizontal orthorhombic layers. The data $\{\tau_Q, \boldsymbol{p}_Q, \boldsymbol{W}_Q\}$ were generated for nine common midpoints and contaminated by Gaussian noise with standard deviations of 1% for the zero-offset traveltimes and horizontal slownesses and 2% for the matrices $\mathbf{W}$ describing the NMO ellipses. After fixing the interval vertical velocities $V_{P0,n}$, $V_{S0,n}$ ($n = 1, 2, 3$) at the correct values, we performed the inversion for the interval anisotropic coefficients, the azimuths β_n of the vertical symmetry planes and the layer thicknesses. Knowledge of the vertical velocities ensures that all anisotropic coefficients except for $\delta^{(3)}$ are estimated with high accuracy. The parameter $\delta^{(3)}$ has no influence on the NMO ellipses of both P- and S-waves in a horizontal orthorhombic layer (Grechka et al., 1999), so it is not constrained by the input data. The standard deviations in the azimuths of the symmetry planes do not exceed 1°, and the deviations in the layer thicknesses are less than 1%.

Application of our tomographic algorithm to a more complicated layered model with curved interfaces is illustrated by Figure 7. The input data were computed again for nine common midpoints (Figure 7a) and contaminated by Gaussian noise with the same standard deviations as in Figure 6. In addition to the interval anisotropic parameters and the azimuths β_n of the vertical symmetry planes, the algorithm was designed to reconstruct the shapes of all three interfaces. As expected for any technique based on surface traveltime data, parameter estimation becomes less stable with depth (Figures 7b,c,d). Nevertheless, the standard deviations in the anisotropic parameters do not exceed 0.1 (the value for $\delta_3^{(1)}$ in Figure 7d). Taking into account that the error amplification for a given layer is proportional to its relative thickness, we conclude that the anisotropic coefficients are constrained reasonably well. The azimuths of the symmetry planes and the shapes of the interfaces were also estimated with high accuracy; the standard deviations in β_1, β_2 and β_3 are 1.0°, 1.6° and 4.6°, respectively.

5 DISCUSSION AND CONCLUSIONS

Estimating the parameters of orthorhombic media from surface seismic data is of primary importance in building realistic models of naturally fractured reservoirs. We demonstrated that 3-D multiazimuth reflection moveout of PP-waves and two split SS-waves on conventional-length spreads can be used to reconstruct orthorhombic velocity fields in the depth domain. The SS traveltimes can be computed from PP and converted PS data using the model-independent method of Grechka and Tsvankin (2001), so excitation of shear waves is not necessary. Then the NMO ellipses, zero-offset traveltimes and re-

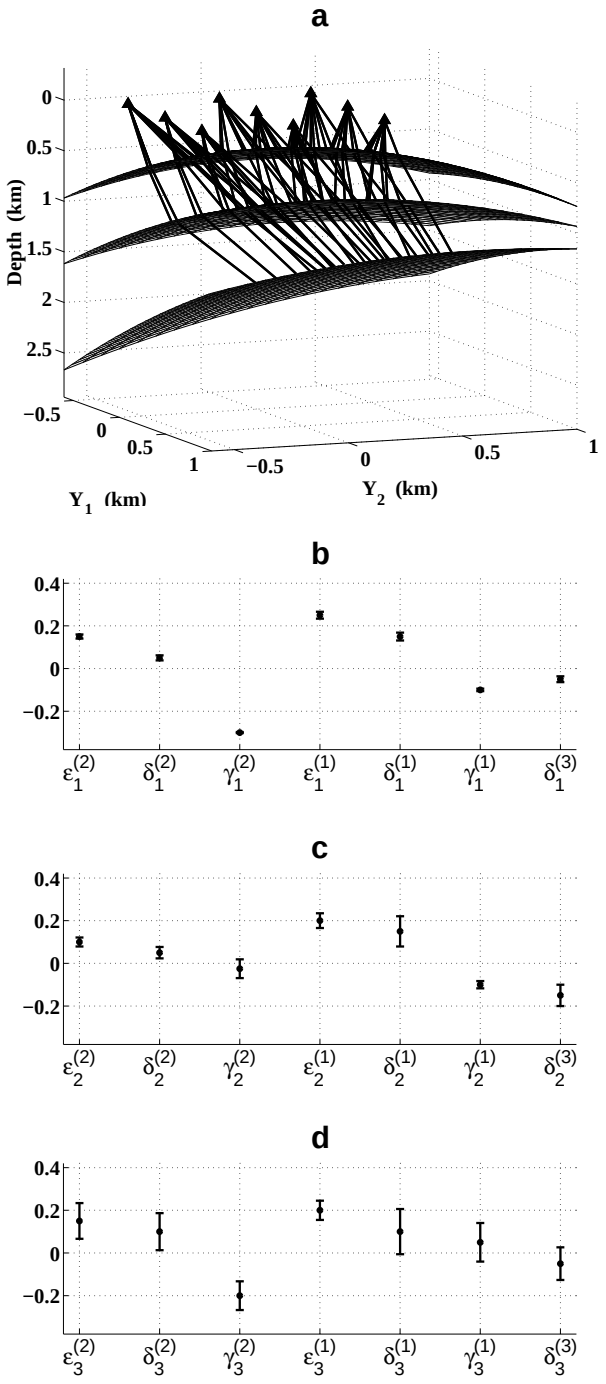

Figure 7. (a) Reflected zero-offset rays of the P-, S_1- and S_2-waves in a three-layer orthorhombic medium, and (b,c,d) the results of stacking-velocity tomography. The vertical velocities $V_{P0,1} = 1.0$ km/s, $V_{S0,1} = 0.6$ km/s, $V_{P0,2} = 1.5$ km/s, $V_{S0,2} = 0.8$ km/s, and $V_{P0,3} = 1.8$ km/s, $V_{S0,3} = 1.0$ km/s were assumed to be known. The azimuths of the symmetry planes are $\beta_1 = 40°$, $\beta_2 = 50°$ and $\beta_3 = 10°$.

flection slopes of the PP- and SS-waves are inverted for the interval anisotropic parameters and the shapes of the interfaces (we call this approach "stacking-velocity tomography").

The theoretical conditions needed to make this inversion unique require that the reflector has at least a mild dip (ϕ) and the azimuth of the dip plane (ψ) be different from those of the vertical symmetry planes of the overburden ($\beta \pm 90°$). If the reflector is horizontal, the vertical velocities and the anisotropic parameters $\epsilon^{(1,2)}$, $\delta^{(1,2,3)}$ and $\gamma^{(1,2)}$ cannot be obtained from the reflection traveltimes of PP- and SS-waves (or PS-waves) alone (Grechka, Theophanis and Tsvankin, 1999). Even a mild reflector dip $\phi = 15 - 20°$, however, makes the inversion for a single orthorhombic layer feasible; a similar result was obtained by Tsvankin and Grechka (2000a,b) for VTI media.

When the dip plane of the reflector coincides with one of the vertical symmetry planes of the overburden, the NMO ellipses are co-oriented with the dip and strike directions and do not contain enough information about the medium parameters. The difference between the dip direction and the azimuth of the nearest symmetry plane has to exceed 10° to ensure unambiguous inversion. The same condition ($|\psi - \beta| > 10°$) is required in the inversion of multiazimuth PP-wave traveltimes for the anellipticity parameters η of orthorhombic media (Grechka and Tsvankin, 1999a).

A number of synthetic tests on noise-contaminated data for typical orthorhombic models shows that for a single layer noise does not get amplified by the inversion algorithm. In contrast, the estimated anisotropic parameters in layered orthorhombic media often are significantly distorted as a result of error accumulation with depth and a reduced sensitivity of surface data to the parameters of deeper layers. We suggested to avoid this instability in stacking-velocity tomography by supplementing the surface data with the vertical velocities of the P- and S-waves measured from well logs or check shots. This constraint makes the inversion results sufficiently stable for application in quantitative fracture characterization for orthorhombic reservoir models (Bakulin et al., 2000).

6 ACKNOWLEDGMENTS

We thank Ken Larner and Kumar Gautam for reviewing the manuscript.

7 REFERENCES

Alford, R.M., 1986, Shear data in the presence of azimuthal anisotropy: 56th Ann. Internat. Mtg., Soc. Expl. Geophys., Expanded Abstracts, 476–479.

Alkhalifah, T., and Tsvankin, I., 1995, Velocity analysis in transversely isotropic media: Geophysics, **60**, 1550–1566.

Bakulin, A., Grechka, V., and Tsvankin, I., 2000, Estimation of fracture parameters from reflection seismic data – Part II: Fractured models with orthorhombic symmetry: Geophysics, **65**, 1803–1817.

Grechka, V., Contreras, P., and Tsvankin, I., 2000, Inversion of normal moveout for monoclinic media: Geophysical Prospecting, **48**, 577–602.

Grechka, V., Pech, A., and Tsvankin, I., 2001, Multicomponent stacking-velocity tomography for transversely isotropic media: CWP Project Review (CWP-365).

Grechka, V., Pech, A., and Tsvankin, I., 2002, P-wave stacking-velocity tomography for VTI media: Geophys. Prosp., **50**, 151–168.

Grechka, V., Theophanis, S., and Tsvankin, I., 1999, Joint inversion of P- and PS-waves in orthorhombic media: Theory and a physical-modeling study: Geophysics, **64**, 146–161.

Grechka, V., and Tsvankin, I., 1998a, Feasibility of non-hyperbolic moveout inversion in transversely isotropic media: Geophysics, **63**, 957-969.

Grechka, V., and Tsvankin, I., 1998b, 3-D description of normal moveout in anisotropic inhomogeneous media: Geophysics, **63**, 1079-1092.

Grechka, V., and Tsvankin, I., 1999a, 3-D moveout velocity analysis and parameter estimation for orthorhombic media: Geophysics, **64**, 820–837.

Grechka, V., and Tsvankin, I., 1999b, 3-D moveout inversion in azimuthally anisotropic media with lateral velocity variation: Theory and a case study: Geophysics, **64**, 1202–1218.

Grechka, V., and Tsvankin, I., 2001, $PP + PS = SS$: CWP Project Review (CWP-347P).

Grechka, V., Tsvankin, I., Bakulin, A., and Hansen, J.O., 2001, Joint inversion of PP and PS reflection data for VTI media: A North Sea case study: CWP Project Review (CWP-366).

Le Stunff, Y., Grechka, V., and Tsvankin, I., 2001, Depth-domain velocity analysis in VTI media using surface P-wave data: Is it feasible?: Geophysics, **66**, 897–903.

Schoenberg, M., and Helbig, K., 1997, Orthorhombic media: Modeling elastic wave behavior in a vertically fractured earth: Geophysics, **62**, 1954–1974.

Thomsen, L., 1986, Weak elastic anisotropy: Geophysics, **51**, 1954–1966.

Thomsen, L., 1999, Converted-wave reflection seismology over inhomogeneous, anisotropic media: Geophysics, **64**, 678–690.

Tsvankin, I., 1997, Anisotropic parameters and P-wave velocity for orthorhombic media: Geophysics, **62**, 1292–1309.

Tsvankin, I., 2001, Seismic signatures and analysis of reflection data in anisotropic media: Elsevier Science.

Tsvankin, I., and Grechka, V., 2000a, Dip moveout of converted waves and parameter estimation in transversely isotropic media: Geophysical Prospecting, **48**, 257–292.

Tsvankin, I., and Grechka, V., 2000b, Two approaches to anisotropic velocity analysis of converted waves: 70th Ann. Internat. Mtg., Soc. Expl. Geophys., Expanded Abstracts, 1193–1196.